

Spin hydrodynamic generation

R. Takahashi^{1,2,3,4*}, M. Matsu^{2,4}, M. Ono^{2,4}, K. Harii^{2,4}, H. Chudo^{2,4}, S. Okayasu^{2,4}, J. Ieda^{2,4}, S. Takahashi^{1,4}, S. Maekawa^{2,4} and E. Saitoh^{1,2,3,4*}

Magneto-hydrodynamic generation¹⁻⁴ is the conversion of fluid kinetic energy into electricity. Such conversion, which has been applied to various types of electric power generation, is driven by the Lorentz force acting on charged particles and thus a magnetic field is necessary^{3,4}. On the other hand, recent studies of spintronics⁵⁻²³ have revealed the similarity between the function of a magnetic field and that of spin-orbit interactions in condensed matter. This suggests the existence of an undiscovered route to realize the conversion of fluid dynamics into electricity without using magnetic fields. Here we show electric voltage generation from fluid dynamics free from magnetic fields; we excited liquid-metal flows in a narrow channel and observed longitudinal voltage generation in the liquid. This voltage has nothing to do with electrification or thermoelectric effects, but turned out to follow a universal scaling rule based on a spin-mediated scenario. The result shows that the observed voltage is caused by spin-current⁶ generation from a fluid motion: spin hydrodynamic generation. The observed phenomenon allows us to make mechanical spin-current and electric generators, opening a door to fluid spintronics.

An electron is an elementary particle which carries internal angular momentum called an electron spin. The recent development of nanotechnology has enabled spins to be used to form a new field called spintronics. Various phenomena found in spintronics originate from angular-momentum exchange between the spin and other degrees of freedom, such as magnetization^{7,8} and light polarization⁹⁻¹¹; so far, many degrees of freedom have been united into this angular-momentum exchange framework. However, the exchange has not been observed for the most common and ordinary carrier of angular momentum—namely, mechanical rotation of material objects.

The interaction which combines mechanical angular momentum and electron spin is called spin-rotation coupling^{12,13}. With this coupling, mechanical rotation gives rise to spin voltages and spin currents. Here, the spin voltage is the driving force for a spin current, represented by $\mu^s \equiv \mu_\uparrow - \mu_\downarrow$, where μ_\uparrow and μ_\downarrow respectively denote the electrochemical potential for spin-up and spin-down electrons^{16,17}; a gradient of spin voltage drives a spin current.

To generate a gradient of spin voltage from mechanical motion, we have used flows of a liquid metal (Fig. 1a), as a gradient of mechanical rotation can easily be generated in a fluid. To describe spin voltage generation in a liquid, we expanded the angular-momentum conservation law for fluid dynamics to include angular-momentum transfer between a liquid and an electron spin. By introducing an antisymmetric stress tensor to the equation of motion for a liquid, the angular momentum of a fluid is predicted to be transferred into the electron spin (see Supplementary

Information for details). The obtained equation for the spin voltage μ^s (the vector indicates a polarized direction) is

$$\nabla^2 \mu^s = \frac{1}{\lambda^2} \mu^s - \frac{4e^2}{\sigma_0 \hbar} \xi \omega \quad (1)$$

where λ is the spin-diffusion length¹⁸ and ξ is related to the fluid viscosity caused by the angular-momentum transfer, which is added to the viscosity coefficient of a Newtonian fluid. The vorticity²⁴ $\omega \equiv \text{rot } \mathbf{v}$ represents local mechanical rotation of a fluid, where \mathbf{v} is the fluid velocity (Fig. 1b). Equation (1) implies that the vorticity acts as a spin-current source (Fig. 1c).

To detect spin voltage in a fluid, we have used the inverse spin Hall effect^{17,19-22} (ISHE). The ISHE converts a spin current into an electric field \mathbf{E}_{ISHE} through the spin-orbit interaction of electrons. The spin current \mathbf{j}^s carries the spin σ . The relationship between \mathbf{E}_{ISHE} and \mathbf{j}^s is given by

$$\mathbf{E}_{\text{ISHE}} = -\frac{2|e|}{\sigma_0 \hbar} \theta_{\text{SHE}} \mathbf{j}^s \times \sigma \quad (2)$$

where σ_0 and θ_{SHE} are the electrical conductivity and the spin Hall angle, respectively. By measuring \mathbf{E}_{ISHE} , the ISHE can be used to detect a spin current precisely (see Fig. 1d).

Figure 1e shows the geometry for mechanical spin-current generation in a cylindrical fluid channel used in the present study. In the channel, the vorticity ω is generated as a result of the viscosity near the inner wall and lies along the azimuthal direction (θ). Therefore, equations (1) and (2) predict a spatial gradient of μ^s along the radial direction (r) and the generation of \mathbf{E}_{ISHE} due to the ISHE of a liquid metal along the axial direction (z).

Figure 2a shows a schematic illustration of the measurement set-up. In this set-up, we generate a flow of liquid metal mercury (Hg) in a cylindrical channel by applying a pulsed pressure ΔP . The channels consist of a quartz pipe and platinum (Pt) thin wires as electrodes embedded in the channel wall and electrically connected to the liquid metal via a pinhole to avoid disturbance of the fluid flow. The channel has to be an insulator for spin hydrodynamic (SHD) measurements to avoid thermoelectric effects between the channel and the liquid metal. The electrode material is chosen as Pt because of its weak chemical reactivity and its absolute thermopower being close to that of Hg; the observed relative Seebeck coefficient is $S_{\text{Hg-Pt}} = +0.06 \mu\text{V K}^{-1}$. The inner diameter and the length of the channel (the distance between the electrodes) are denoted as ϕ and L , respectively. To prevent it from charging up electrically, the Hg is connected to the ground at the inlet. We measured the electric voltage difference V between the ends of the channel filled with Hg. All the measurements were performed at room temperature.

¹Institute for Materials Research, Tohoku University, Sendai 980-8577, Japan. ²Advanced Science Research Center, Japan Atomic Energy Agency, Tokai 319-1195, Japan. ³WPI Research Center, Advanced Institute for Material Research, Tohoku University, Sendai 980-8577, Japan. ⁴ERATO, Japan Science and Technology Agency, Sendai 980-8577, Japan. *e-mail: r.takahashi@imr.tohoku.ac.jp; eizi@imr.tohoku.ac.jp

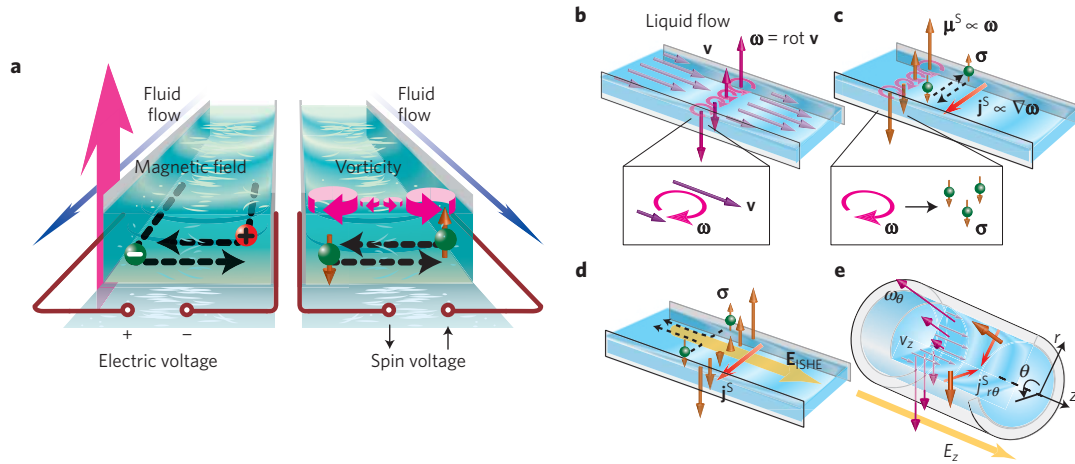


Figure 1 | Concept of spin hydrodynamic generation. **a**, Schematic illustrations of conventional magnetohydrodynamic generation (left) and spin hydrodynamic generation (right). The left panel shows that a fluid flow in a magnetic field generates an electric voltage perpendicular to the flow. The right panel shows that a liquid-metal flow generates a spin voltage, the driving force for a spin current, along the vorticity gradient. **b**, Schematic illustration of the velocity \mathbf{v} and vorticity $\boldsymbol{\omega}$ distribution in a liquid flow confined in a channel. A translational motion with different \mathbf{v} in a local region of a flow exhibits local rotational motion, whose angular velocity is proportional to $\boldsymbol{\omega} \equiv \text{rot } \mathbf{v}$. **c**, Schematic illustration of the mechanically induced spin voltage $\boldsymbol{\mu}^S$ and spin current \mathbf{j}^S . A diffusive spin current flows along the gradient of $\boldsymbol{\mu}^S$, or $\boldsymbol{\omega}$. **d**, Schematic illustration of the inverse spin Hall effect (ISHE) in the fluid. \mathbf{E}_{ISHE} denotes an electric field. **e**, Schematic illustration of mechanical spin-current generation in a cylindrical fluid channel. $v_z, \omega_\theta, j_{r\theta}^S$ and E_z are, respectively, the flow velocity, the vorticity, the mechanically induced spin current [$j_{r\theta}^S \equiv -(\sigma_0 h/4e^2)(\partial/\partial r)\mu_\theta^S$] and the ISHE electric field. $\boldsymbol{\omega}$ is along an azimuthal direction (θ) and has its spatial gradient along a radial direction (r). A spin current induced by the gradient of ω_θ flows along the r -direction.

Figure 2b shows the time evolution of V measured in the liquid Hg. The liquid flow in the channel starts at time $t = 0$ and ends at $t = \Delta t$. A clear V signal appears when Hg is flowing, as shown in Fig. 2b. The sign of V is reversed on reversing the flow direction. This unconventional voltage behaviour is the feature predicted for the ISHE induced by a mechanical motion described above: the direction of \mathbf{E}_{ISHE} is predicted to be reversed by reversing the $\boldsymbol{\omega}$ direction or the Hg flow direction (see Fig. 1e and equation (2)).

To further examine the voltage generation, we measured V for various values of mean flow velocity, v , and for several channels with different ϕ and L values. v is modulated by changing ΔP ; the measurement result, shown in Fig. 2c, is reproduced well by the relation for a turbulent flow in a pipe²⁴, being consistent with the fact that its Reynolds number, Re ($=v\phi/\nu$), satisfies the turbulent flow condition, $4,000 < Re < 10,000$, where ν is the kinetic viscosity. The time evolution of V shown in Fig. 2d clearly illustrates that the magnitude of V increases with increasing ΔP , or the mean flow velocity v . Figure 2e shows the friction velocity²⁴ (v_*) dependence of V for channels with different ϕ and L values. The result shows that V increases with v_* but with different slopes for the different channels. Here, v_* is directly related to the $\boldsymbol{\omega}$ gradient in a turbulent flow: the vorticity of a turbulent flow, $\omega_\theta(r)$, in a pipe is described²⁴ by $\omega_\theta(r) = v_*^2/\nu$ in the region close to the wall, called the viscous sublayer, with $\omega_\theta(r) = v_* / [\kappa(r_0 - r)]$ elsewhere. κ is the von Kármán constant and $r_0 \equiv \phi/2$. The relationship between v_* and v for different ϕ is shown in the inset to Fig. 2f, which was calculated²⁴ by averaging the velocity distribution of the turbulent flow in the pipe.

In this way, different channels were found to exhibit different V behaviour. However, we predict a scaling rule on the behaviour as follows. A spin voltage can be generated from $\omega_\theta(r)$ as a result of the spin-rotation coupling, and the spatial gradient of the spin voltage is then converted into spin currents in the liquid metal and into an electric voltage via the ISHE:

$$V = \left(\frac{L}{r_0^3}\right) C_0 \left[\frac{(v_* r_0)^2}{\nu \mathcal{R} e^\delta} - (v_* r_0) \ln \frac{(v_* r_0)}{\nu \mathcal{R} e^\delta} - (v_* r_0) \right] \quad (3)$$

where $C_0 \equiv (4|e|/\kappa\hbar)((\theta_{\text{SHE}}\lambda^2\xi)/\sigma_0)$, $\mathcal{R}e^\delta \equiv v_* r_0/\nu$ ($\simeq 11.6$ for the present study), and δ_0 is the thickness of the viscous sublayer (see Supplementary Information for detailed derivation). This formula predicts that $r_0^3 V/L$ exhibits a universal scaling with respect to $v_* r_0$, identifying that the V signal is generated from the spin current.

In Fig. 2f, we replot all the data from Fig. 2e for different channels into a $r_0^3 V/L$ versus $v_* r_0$ scale. In this plot, surprisingly, all the different data collapse onto a single curve. This universal scaling behaviour is the very feature predicted above (equation (3)), demonstrating that the observed V signal is due to the ISHE induced by mechanically generated spin currents.

By fitting the data in Fig. 2f with equation (3), the parameter $\theta_{\text{SHE}}\lambda^2\xi$ is estimated to be $5.9 \times 10^{-25} \text{ J s m}^{-1}$. If we assume typical magnitudes^{18,23} of θ_{SHE} and λ ($\theta_{\text{SHE}} \sim 10^{-2}$ and $\lambda \sim 10^{-8} \text{ m}$), ξ is then estimated to be $6 \times 10^{-7} \text{ J s m}^{-3}$, or $\xi/\mu \sim 4 \times 10^{-4}$, where μ is the Newtonian viscosity. Here, we used parameters from ref. 24 for Hg: $\sigma_0 = 1.01 \times 10^6 (\Omega \text{ m})^{-1}$, $\nu = 1.2 \times 10^{-7} \text{ m}^2 \text{ s}^{-1}$ and $\mu = 1.6 \times 10^{-3} \text{ J s m}^{-3}$.

We also carried out measurements on $\text{Ga}_{62}\text{In}_{25}\text{Sn}_{13}$ (GaInSn), another chemically stable liquid metal (melting point: 5°C), whose spin-orbit coupling may be weaker than that in Hg because all atoms comprising GaInSn are lighter than Hg. In the measurements, because an appropriate material is not available for the electrode in GaInSn, we used a special set-up, called a triangle set-up; the details of the set-up are explained later. Figure 3a shows the ΔP dependence of v in GaInSn and Hg. The velocity of GaInSn is faster than that in Hg because of the density difference. Figure 3b,c shows v_* versus V plots of GaInSn and Hg, and the time evolution of V for various values of ΔP in GaInSn, respectively. The data show that V is slightly suppressed by substituting Hg for GaInSn. Equations (1) and (2) phenomenologically indicate that the conversion from the vorticity into the voltage depends on θ_{SHE} and λ . When spin-orbit coupling decreases, θ_{SHE} decreases whereas λ tends to increase. Therefore, the effects of spin-orbit coupling on V partially compensate, resulting in the weak material dependence obtained from the GaInSn and Hg measurements. If we assume $\theta_{\text{SHE}}\lambda^2\xi$ for GaInSn to be $3.0 \times 10^{-24} \text{ J s m}^{-1}$, equation (3) reproduces

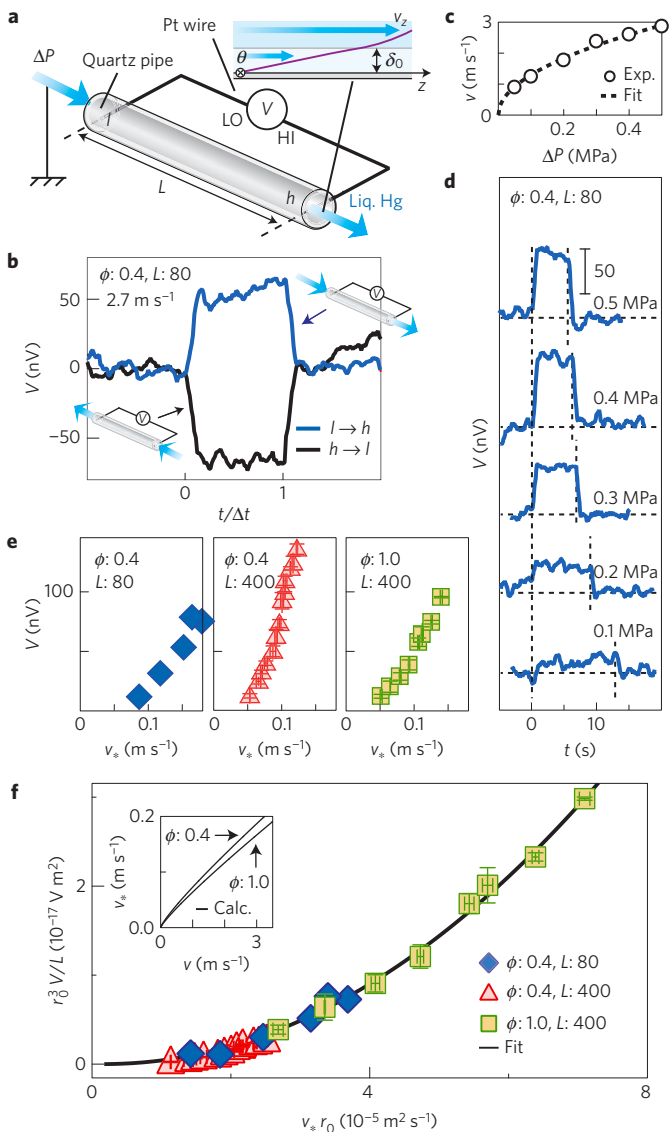


Figure 2 | Electromotive force measurements. **a**, Schematic illustration of the experimental set-up. A flow of liquid Hg is induced by applying a pulsed pressure ΔP . V denotes the electric voltage difference between Pt electrodes (diameter: 0.1 mm) embedded into the channel ends. L (mm) is the distance between the electrodes. The inset shows the velocity v_z distribution²⁴ of turbulent flow in a pipe (see Supplementary Information for details). δ_0 is the thickness of the viscous sublayer. **b**, Time evolution of V for two flow directions: one is a flow injected from the side l (see **a**) and the other is one from the side h . In both cases Hg is connected to the ground at the inlet. The mean flow velocity is 2.7 m s^{-1} . The flow is started at $t=0$ and switched off at $t=\Delta t$ ($=5.9 \text{ s}$). ϕ (mm) is the inner diameter of the channel. **c**, ΔP dependence of the mean flow velocity v for the channel used in **b**. The experimental data (open circles) are reproduced well by a broken curve²⁴ representing $v \propto \sqrt{\Delta P}$. **d**, Time evolution of V for various values of ΔP in the same channel as **b**. **e**, v_* dependence of V for different ϕ and L . In each measurement with $L=80 \text{ mm}$, V was estimated by taking a time average, whereas when analysing the case with $L=400 \text{ mm}$, V was estimated by taking an average of the steep changes of a voltage signal (see **b**) observed on switching on and off the flow. All the measurements for different values of v_* have been carried out more than three times and an average of the results for each v_* is plotted. Error bars are defined as one standard deviation. **f**, $v_* r_0$ dependence of $r_0^3 V / L$. A fit curve is obtained from equation (3). Each error bar was calculated by converting the errors in **e**. Inset shows the relation between v_* and v calculated for different ϕ values.

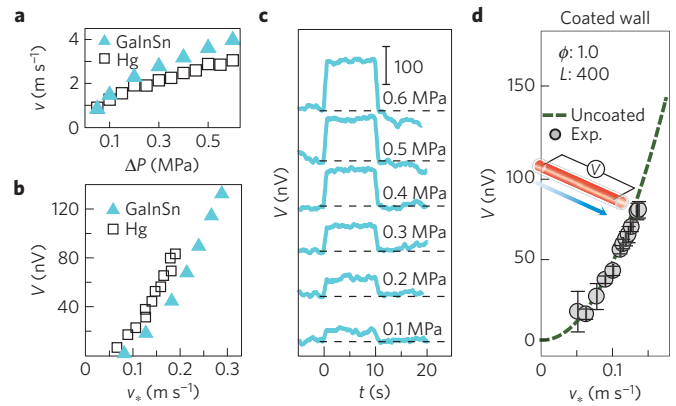


Figure 3 | Experimental results for GalnSn and comparison of voltage with inner-wall material. **a**, ΔP dependences of v for Hg (open symbols) and GalnSn (blue filled symbols) in the triangle set-up shown in Fig. 4a ($\phi=0.4 \text{ mm}$; $L=102 \text{ mm}$). **b**, v_* dependence of V for Hg (open symbols) and GalnSn (blue filled symbols) in the triangle set-up. **c**, Time evolution of V of a GalnSn flow for various values of ΔP . The flow starts at $t=0$ and is switched off at $t=10 \text{ s}$. **d**, Examination of the influence of contact electrification. The v_* dependence of V for the channel whose inner wall is coated with resin (filled circles) exhibits almost the same behaviour as that for the uncoated quartz pipe (broken curve: a fit curve of the data shown in Fig. 2f). The voltage signal V was estimated in the same way as the uncoated quartz pipe case with $L=400 \text{ mm}$ shown in Fig. 2e. Error bars are defined as one standard deviation.

the observed V values. Here, we used parameters from ref. 25 for GalnSn: $\sigma_0 = 3.1 \times 10^6 \text{ } (\Omega \text{ m})^{-1}$ and $\nu = 2.98 \times 10^{-7} \text{ m}^2 \text{ s}^{-1}$.

Now, we examine the possibilities of other mechanisms that might give rise to voltage signals in the present set-up. First, the magnetohydrodynamic effect^{1–4} (MHD), or the effect of the Lorentz force on a liquid-metal flow caused by environmental magnetic fields, was found to be negligible; the electromotive force caused by the MHD is perpendicular to the liquid flow, and thus the voltage caused by the MHD should not depend on the length of a channel, which is contradictory to the observed signal. Also, we confirmed that the observed signal is not affected by the direction of the geomagnetic field.

Next, we examine contact electrification effects^{26–29}, or the influence of charging effects of Hg due to electrochemical interaction with a channel wall, even though the Hg is connected to the ground. A flow of charged Hg might generate electric voltage in itself. The charging effect is known to depend on the material species^{26–28} and roughness²⁹ of the contact surface. To change the property of the contact surface, we coated the inner wall of the channel with resin and measured V using the coated channel. Resin is known to exhibit different electrification properties from quartz^{26,27}. The values of ϕ and L for the channel are 1.0 mm and 400 mm, respectively. The magnitude of the roughness was also changed approximately from 5 to 40 μm by the coating. As shown in Fig. 3d, the result indicates that the v_* dependence of V for the resin-coated channel is the same as that for the uncoated quartz channel, ruling out the contribution of the charging effect.

Finally, we examine the influence of thermoelectric effects. We constructed the special set-up shown in Fig. 4a. We call it the triangle set-up. This set-up allows us to completely eliminate the Seebeck voltage and to examine thermoelectric contamination in the SHD measurements. In the set-up, the voltage probes consist of Hg itself, allowing the voltage to be transferred to a common location for the attachment of wiring, as shown in Fig. 4a. Therefore, thermoelectric contamination is completely removed as follows. In Fig. 4b, we show the voltage signal generated in the triangle set-up

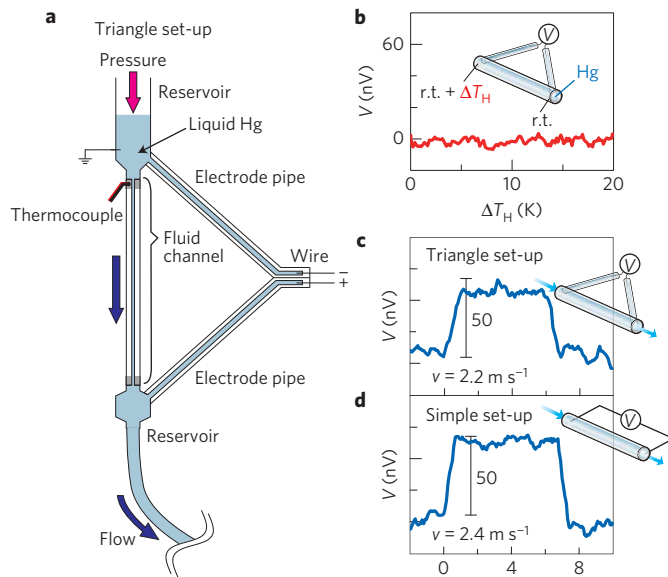


Figure 4 | Measurements in triangle set-up. **a**, Schematic illustration of the triangle set-up, in which liquid-metal electrodes are used. Two quartz pipes (inner diameter: 1.0 mm, length: 100 mm) filled with Hg are used as electrodes. To avoid liquid-flow disturbance, the electrode pipes are connected to liquid reservoirs near the inlet or the outlet of the fluid channel ($\phi = 0.4$ mm, $L = 102$ mm). The other ends of the electrode pipes are placed in close proximity to each other to realize an isothermal condition and are connected to a nanovoltmeter. **b**, Voltage measured without a fluid flow versus temperature difference between the ends of the fluid channel, ΔT_H . The temperature difference is monitored with a T-type thermocouple. r.t. stands for room temperature. **c,d**, Time evolution of the fluid-flow-induced voltage V in the triangle set-up (**c**) and in the simple set-up (**d**). Voltage signals appear when Hg flows with velocity v on applying a pulsed pressure.

filled with Hg, measured by applying a temperature difference ΔT_H between the ends of the fluid channel, but without flowing Hg. The maximum magnitude of ΔT_H is 20 K, much greater than the possible temperature difference in the liquid flow (approximately 0.1 K; see experimental results in Supplementary Information). Note, however, that no noticeable thermoelectric voltage is observed in going from a small to a large ΔT_H , which shows that the thermoelectric effect is completely excluded in measuring the SHD signal. In fact, as shown in Fig. 4c,d, we observed flow-induced voltage signals in the triangle set-up, similar to those in the set-up shown in Fig. 2a (the simple set-up). Compared to this flow-induced signal in the triangle set-up, the thermoelectric signal in Fig. 4b is negligibly small even in the presence of a large temperature difference, proving that both the set-ups work perfectly to measure the SHD signal. To confirm this we compared the flow-induced voltage signal in the triangle set-up shown in Fig. 4c and that in the simple set-up shown in Fig. 4d; they are similar in terms of the flow velocity dependence and the signal magnitude. All the results indicate that the voltage signal generated in the liquid flow is completely unrelated to thermoelectricity.

From the point of view of applications, the observed generation effects can be used to make an electric generator and a spin generator without using magnets. It is thus certainly worthwhile to explore the effect in various liquid metals. We anticipate that the observed phenomena will bridge the gap between spintronics and hydrodynamics.

Received 7 August 2014; accepted 15 September 2015; published online 2 November 2015

References

- Rosa, R. J. *Magnetohydrodynamic Energy Conversion* Ch. 4 (McGraw-Hill, 1968).
- Alfvén, H. Existence of electromagnetic-hydrodynamic waves. *Nature* **150**, 405–406 (1942).
- Michiyoshi, I. & Nakura, S. Pressure drop of liquid mercury MHD power generators. *J. Nucl. Sci. Technol.* **9**, 490–496 (1972).
- Yamaguchi, H., Niu, X.-D. & Zhang, X.-R. Investigation on a low-melting-point gallium alloy MHD power generator. *Int. J. Energy Res.* **35**, 209–220 (2011).
- Maekawa, S. (ed.) *Concepts in Spin Electronics* (Oxford Univ. Press, 2006).
- Maekawa, S., Valenzuela, S. O., Saitoh, E. & Kimura, T. (eds) *Spin Current* (Oxford Univ. Press, 2012).
- Slonczewski, J. C. Current-driven excitation of magnetic multilayers. *J. Magn. Magn. Mater.* **159**, L1–L7 (1996).
- Berger, L. Emission of spin waves by a magnetic multilayer traversed by a current. *Phys. Rev. B* **54**, 9353–9358 (1996).
- Ando, K. et al. Photoinduced inverse spin-Hall effect: Conversion of light-polarization information into electric voltage. *Appl. Phys. Lett.* **96**, 082502 (2010).
- Kimel, A. V. et al. Ultrafast non-thermal control of magnetization by instantaneous photomagnetic pulses. *Nature* **435**, 655–657 (2005).
- Göthgen, C., Oszwaldowski, R., Petrou, A. & Zutti, I. Analytical model of spin-polarized semiconductor lasers. *Appl. Phys. Lett.* **93**, 042513 (2008).
- Matsuo, M., Ieda, J., Saitoh, E. & Maekawa, S. Effects of mechanical rotation on spin currents. *Phys. Rev. Lett.* **106**, 076601 (2011).
- Matsuo, M., Ieda, J., Harii, K., Saitoh, E. & Maekawa, S. Mechanical generation of spin current by spin-rotation coupling. *Phys. Rev. B* **87**, 180402 (2013).
- Uchida, K. et al. Long-range spin Seebeck effect and acoustic spin pumping. *Nature Mater.* **10**, 737–741 (2011).
- Uchida, K., An, T., Kajiwara, Y., Toda, M. & Saitoh, E. Surface-acoustic-wave-driven spin pumping in $Y_3Fe_5O_{12}/Pt$ hybrid structure. *Appl. Phys. Lett.* **99**, 212501 (2011).
- Valet, T. & Fert, A. Theory of the perpendicular magnetoresistance in magnetic multilayers. *Phys. Rev. B* **48**, 7099–7113 (1993).
- Takahashi, S. & Maekawa, S. Spin current in metals and superconductors. *J. Phys. Soc. Jpn* **77**, 031009 (2008).
- Bass, J. & Pratt, W. P. Jr Spin-diffusion lengths in metals and alloys, and spin-flipping at metal/metal interfaces: An experimentalist's critical review. *J. Phys. Condens. Matter* **19**, 183201 (2007).
- Saitoh, E., Ueda, M., Miyajima, H. & Tatara, G. Conversion of spin current into charge current at room temperature: Inverse spin-Hall effect. *Appl. Phys. Lett.* **88**, 182509 (2006).
- Valenzuela, S. O. & Tinkham, M. Direct electronic measurement of the spin Hall effect. *Nature* **442**, 176–179 (2006).
- Kimura, T., Otani, Y., Sato, T., Takahashi, S. & Maekawa, S. Room-temperature reversible spin Hall effect. *Phys. Rev. Lett.* **98**, 156601 (2007).
- Azevedo, A., Vilela Leã, L. H., Rodriguez-Suarez, R. L., Oliveira, A. B. & Rezende, S. M. dc effect in ferromagnetic resonance: Evidence of the spin-pumping effect? *J. Appl. Phys.* **97**, 10C715 (2005).
- Ando, K. et al. Inverse spin-Hall effect induced by spin pumping in metallic system. *J. Appl. Phys.* **109**, 103913 (2011).
- Landau, L. D. & Lifshitz, E. M. *Fluid Mechanics* 2nd edn, Ch. 1, 2 & 4 (Butterworth-Heinemann, 1987).
- Morley, N. B., Burris, J., Cadwallader, L. C. & Nornberg, M. D. GaInSn usage in the research laboratory. *Rev. Sci. Instrum.* **79**, 056107 (2008).
- Shaw, P. E. Experiments on tribo-electricity. I. The tribo-electric series. *Proc. R. Soc. Lond. A* **94**, 16–33 (1917).
- Diaz, A. F. & Felix-Navarro, R. M. A semi-quantitative tribo-electric series for polymeric materials: The influence of chemical structure and properties. *J. Electrostat.* **62**, 277–290 (2004).
- Yarnold, G. D. The electrification of mercury indexes in their passage through tubes. *Proc. Phys. Soc.* **52**, 196–201 (1940).
- Hori, Y. & Saito, K. Effect of the surface roughness on contact charging of polypropylene with mercury. *J. Inst. Electrostat. Jpn* **24**, 42–46 (2000).

Acknowledgements

The authors thank Y. Fujikawa, R. Iguchi, Y. Ohnuma, J. Ohe, R. Haruki, Y. Shiomi, K. Ando, M. Mizuguchi and T. Seki for valuable discussions. This work was supported by ERATO-JST 'Spin Quantum Rectification Project', Japan, a Grant-in-Aid for Scientific Research on Innovative Areas from MEXT, Japan, a Grant-in-Aid for JSPS Fellows from JSPS, Japan, a Grant-in-Aid for Young Scientists B (24740247 and 24760722) from MEXT, Japan, a Grant-in-Aid for Challenging Exploratory Research (26610108) from MEXT, Japan, a Grant-in-Aid for Scientific Research A (24244051 and 26247063) from MEXT, Japan, and a Grant-in-Aid for Scientific Research C (25400337 and 15K05153) from MEXT, Japan.

Author contributions

R.T., M.O., K.H., H.C. and E.S. designed the experiments; R.T., M.O. and K.H. collected and analysed the data; S.O. supported the experiments; R.T., K.H., M.M., J.I. and S.T. developed the theoretical explanations; S.M. and E.S. planned and supervised the study; R.T., E.S., M.M. and J.I. wrote the manuscript; J.I. and E.S. coined the term 'spin hydrodynamic (SHD) generation'. All authors discussed the results and commented on the manuscript.

Additional information

Supplementary information is available in the online version of the paper. Reprints and permissions information is available online at www.nature.com/reprints. Correspondence and requests for materials should be addressed to R.T. or E.S.

Competing financial interests

The authors declare no competing financial interests.